Research Article | Vol. 12, No. 11 / 1 Nov 2021 / Biomedical Optics Express 7051
Biomedical Optics EXPRESS

Nb_2CT_x MXene-tilted fiber Bragg grating optofluidic system based on photothermal spectroscopy for pesticide detection

WENJIE LI,[1] YINPING MIAO,[1,*] TUAN GUO,[2] KIALIANG ZHANG,[1] AND JIANQUAN YAO[3]

[1]Tianjin Key Laboratory of Film Electronic and Communicate Devices, School of Integrated Circuit Science and Engineering, Tianjin University of Technology, Tianjin 300384, China
[2]Institute of Photonics Technology, Jinan University, Guangzhou 510632, China
[3]College of Precision Instruments and Opto-Electronics Engineering, Institute of Laser and Optoelectronics, Tianjin University, Tianjin 300072, China
*kikosi@126.com

Abstract: An optofluidic system based on photothermal spectroscopy is proposed, which combines molecular photothermal effect with Nb_2CT_x MXene-tilted fiber Bragg grating (TFBG) for the detection of organophosphorus pesticides (OPs) with temperature compensated. Under the irradiation of excitation light, the photothermal effect of OPs produces a detectable change in the refractive index of the sample, and the concentration of chlorpyrifos can be quantified using TFBG. The Nb_2CT_x MXene coated TFBG allow more molecules to be absorbed on the surface of TFBG, which enhances the interaction between light and matter, and improves the sensitivity of detection. The temperature compensation is performed by referring to the core mode of TFBG, thereby eliminating the influence of ambient temperature on the photothermal detection. The experimental results show that the sensitivity reaches 1.8 pm/ppm with a limit of detection (LOD) of 0.35 ppm, and the obtained temperature compensation coefficient is 4.84 ppm/°C. This photothermal biosensor has the advantages of low LOD, temperature compensation and real-time online monitoring, making it a good candidate in medicine, chemistry and environmental monitoring.

1. Introduction

Organophosphate pesticides (OPs) are phosphorus-containing organic compounds. Due to their high efficiency, low cost, wide range and low harm, OPs are widely used in agricultural planting to prevent the proliferation of pests [1]. However, the problem of excessive pesticide residues poses a serious threat to humans, and causes certain pollution to the environment. Studies have shown that OPs will cause acute cholinergic neurotoxicity even at nanomolar concentration levels, and acute poisoning or long-term exposure to subclinical OPs can produce some long-term neurotoxic consequences [2,3]. In addition, carcinogenic bacteria may be present in soil contaminated by OPs [4,5]. Therefore, it is necessary to real-time and accurate monitor the concentration of pesticide residues in food and agricultural samples.

Currently, the different techniques for pesticide detection mainly include gas chromatography-mass spectrometry (GC-MS) [6,7], high performance liquid chromatography (HPLC) [8,9], electrochemistry [10–12] and surface plasmon resonance (SPR) [13,14]. These are often complicated operation, susceptible electromagnetic interference, and low sensitivity. Compare with the conventional way, photothermal spectroscopy (PTS) exhibits higher sensitivity and selectivity. This is due to the photonically activated thermal signal only comes from the optical absorption of analyte at a specific wavelength, which effectively avoids the influence of scattering and reflection losses on the measured signal [15]. A method utilizes photothermal detection

#442602 https://doi.org/10.1364/BOE.442602
Journal © 2021 Received 8 Sep 2021; revised 3 Oct 2021; accepted 3 Oct 2021; published 22 Oct 2021

Biomedical Optics EXPRESS

based on thermal lens spectroscopy has been proposed to measure low-concentration pesticides in vegetable samples [16]. The photon excites the analyte to yield a detectable change in the refractive index (RI) of sample, and the disturbance of the probe light can provide the concentration information of the analyte. It has the advantages of low cost and no sample pretreatment, but the complex optical path needs to construct and is susceptible to external interference.

In recent years, optical fiber sensors have attracted the attention of researchers due to their anti-electromagnetic interference, simple structure, label-free and real-time detection characteristics. Tilted fiber Bragg grating (TFBG) biosensor have been proved as good platform for the detection of specific molecules in the fields of disease diagnosis, gas monitoring and PH assessment, because its unique properties of high sensitivity, robustness and temperature insensitivity provided by the reference of core mode [17–19]. TFBG is a special short-period fiber Bragg grating (FBG) written with a small tilt angle. In TFBG, a series of cladding modes are sensitive to the change of surrounding environments, so it is a feasible choice for detecting physical or biochemical quantities. More importantly, the core mode is also sensitive to temperature compared with other optical fiber, which resulting in the influence of ambient temperature can be eliminated while detecting biomolecules. The sensitivity in low RI region can be improved by increasing the tilt angle, coating the metal film to excite SPR, or integrating two-dimensional materials [20–22]. MXene is a two-dimensional transition metal carbide similar to graphene. Its molecular formula is $M_{n+1}X_nT_x$, where M is a transition metal, X is C or N, and T_x is a surface functional group [23]. MXene has been widely used in the field of biosensing due to its unique physical and chemical characteristics. The layered structure of MXene makes it have a larger specific surface area, which can increase the contact area with external substances, thereby adsorbing more biomolecules and improving the sensitivity of detection. The functional groups of MXene nanosheets surface, such as =O, -OH, and -F, exhibiting good hydrophilicity that effectively improve the capture of water molecules, and also enhance the detection of biomolecules in the solution [24–26]. Consequently, it is a promising approach that MXene integrated with TFBG to enhance the interaction between light and matter and improve the sensing performance.

In this paper, the niobium carbide (Nb_2CT_x) MXene-TFBG was utilized to detect the concentration of OP (chlorpyrifos) based on the molecular photothermal effect. Under the irradiation of excitation light, the photothermal signal produced by chlorpyrifos absorbing the photon energy changes the RI of the analyte, leading to the changes in the resonance wavelength and intensity of the TFBG cladding modes. Nb_2CT_x MXene is coated on the surface of TFBG by optical deposition method. Its large specific surface area and biocompatibility allow chlorpyrifos molecules to be adsorbed on the surface and enhance the light-matter interaction. The influence of ambient temperature can be eliminated by monitoring the core mode of TFBG. Combining the photothermal detection method with Nb_2CT_x MXene-TFBG shows high sensitivity, temperature compensation, no pretreatment and online label-free detection of chlorpyrifos. Therefore, the proposed photothermal biosensor can be utilised in the fields of food safety monitoring and disease diagnosis.

2. Materials and methods

2.1. Fabrication of the MXene-TFBG biosensor

The TFBG with a tilted angle of 16° is prepared by the phase mask method whose transmission spectrum has the largest resonance amplitude within the refractive index range of the liquid (1.32–1.42). The 16°-tilted TFBG was fixed in the flow cell with UV glue, and the Nb_2CT_x MXene nanosheets (Nanjing Xianfeng Nano Material Technology Co. Ltd.) were coated on the TFBG sensing area with the optical deposition method. The dimension of the flow channel in the PMMA-based microfluidic chip is 40 mm × 4 mm × 2 mm. There are two small holes on the

Biomedical Optics EXPRESS

outside of the channel as the inlet/outlet of the liquid, and the other hole in the middle is used to pass the laser into the channel to excite the photothermal effect of the molecules.

2.2. Detection principle

The incident light guided by the core interacts with the permanently modulated grating, and the tilt of the grating plane direction makes the light satisfying the phase matching condition couple to the core and cladding modes that propagate backward, as shown in Fig. 1(a). A large number of cladding modes correspond to specific resonance wavelengths, leading a resonant comb in the transmission spectrum of the grating. Part of the light transmitted in the cladding mode leaks outside the cladding boundary to form an evanescent field, which is sensitive to changes in the surrounding environment [27]. The effective RI of the cladding mode changes with the environmental RI, resulting in a shift in the resonance wavelength of the corresponding cladding mode (Fig. 1(b)). The boundary between the guided mode and the leakage mode is called the "cut-off" point (the black arrows marked in Fig. 1(b)), where the evanescent field penetrates the external medium to the greatest extent and therefore has the highest sensitivity [28]. The core mode is confined inside the fiber, thus it is less disturbed by the environmental RI. The resonance wavelengths of the core mode λ_{Bragg} and the ith cladding mode $\lambda_{clad,i}$ can be expressed as [29]

$$\lambda_{Bragg} = 2n_{eff}^{core}\frac{\Lambda}{cos\theta} \tag{1}$$

$$\lambda_{clad,i} = (n_{eff}^{clad,i} + n_{eff}^{core})\frac{\Lambda}{cos\theta} \tag{2}$$

where n_{eff}^{core} is the effective RI of the core mode, $n_{eff}^{clad,i}$ is the effective RI of the ith cladding mode. Λ is the period of the grating, and θ is the tilted angle between the grating plane the vertical plane of the fiber. The sensing capability of TFBG can be improved through the mode selection mechanism. After linearly polarized light enters the TFBG, there are two cladding modes in the fiber: the polarization mode parallel to the grating plane (P-mode) and perpendicular to the grating plane (S-mode). Figure 1(c) shows the horizontal component of the P-mode and S-mode transverse electric fields obtained by COMSOL simulation.

$$R = tanh^2(kL) \tag{3}$$

The resonance intensity R of the cladding mode is related to the coupling coefficient k of the core and cladding modes, and also depends on the length L of the grating region of the TFBG. The coupling coefficient decreases with the increase of environmental RI, resulting in a decrease in resonance intensity.

Photothermal technique depends on the absorption of optical radiation by the analyte, which is provided by a laser source. The subsequent non-radiative relaxation of the sample absorbs photonic energy to generate heat, resulting in the rise of sample's temperature (10^{-4}– 10^{-3} K) to yield a detectable change in RI. The relationship between the RI of the analyte and its concentration and temperature is expressed as [30]

$$n = n_0 + \alpha C + \beta T \tag{4}$$

where n_0 is the RI of the solvent, and α, β are the concentration and temperature coefficient of the analyte RI, respectively. The concentration coefficient of the chlorpyrifos RI is small, so the change of its RI is mainly attribute to temperature. The change of temperature caused by the photothermal of the analyte are given by [31]

$$\Delta T = \eta P_{exc} t[1 - exp(-\varepsilon(\lambda_{exc})CD_{eff})] \tag{5}$$

It can be seen that the change of temperature ΔT is determined by multiple parameters. η is the part of the absorbed laser power converted to heat energy. P_{exc} is the laser power that excites the

Biomedical Optics EXPRESS

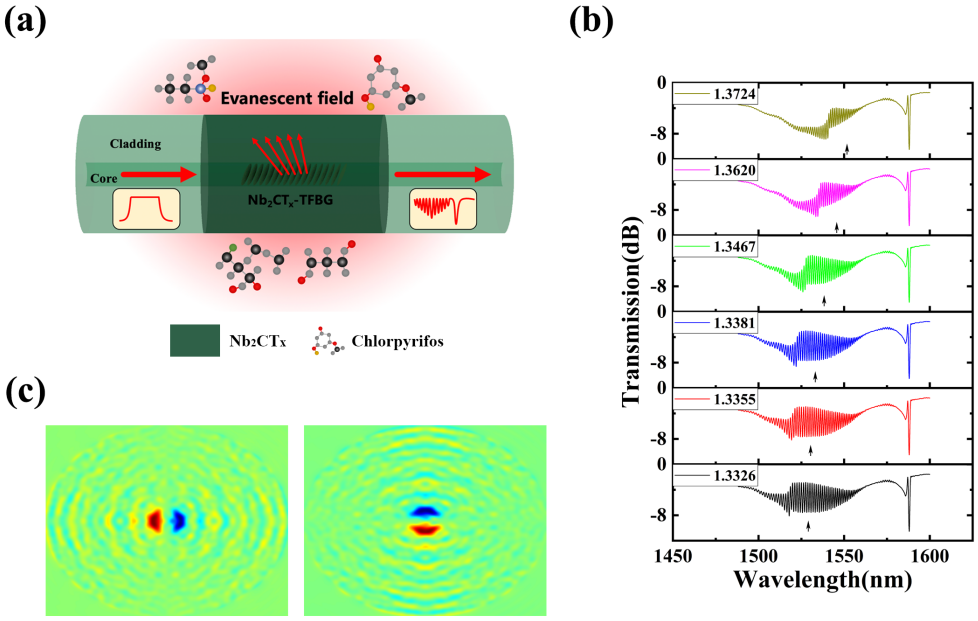

Fig. 1. (a) Schematic diagram of TFBG biosensor. (b) Transmission spectrum of 16° TFBG under different RI. (c) Simulated horizontal component of the P-mode and S-mode transverse electric fields close to "cut-off".

molecular photothermal effect, and t is the irradiation time. ε is the molar absorption coefficient for excitation light with a specific wavelength λ_{exc}, C is the concentration of the analyte, and D_{eff} is the effective depth of the solution. We can conclude from Eq. (5) that when the analyte and the excitation light are determined, the change of temperature caused by the molecular photothermal effect is only related to P_{exc}, t and C. The thermal signal during excitation light irradiation can be enhanced by increasing P_{exc} and t, leading to a detectable change of sample's RI, and realize the quantification of the analyte concentration.

2.3. Experiment setup for pesticide detection

In the experiment, the Nb_2CT_x MXene-TFBG was fixed in the microfluidic channel. A peristaltic pump was used to inject the chlorpyrifos sample solution (Shanghai Aladdin Chemistry Co. Ltd.) into the microfluidic chip to avoid the influence of the external environment on the sample detection. The 400 nm laser source (Changchun New Industries Optoelectronics Technology Co. Ltd., spot diameter: 3.5 mm) was used as an excitation light source to irradiate the analyte through a focusing lens to produce photothermal effect and change the RI of the solution. A supercontinuum broadband source (SBS, SuperK COMPACT, NKT Photonics) was used to excite the sensing TFBG, and the output light was detected by an optical spectrum analyzer (OSA, AQ6317C, Yokogawa). The minimum wavelength resolution is 0.02 nm. The linear polarizer and polarization controller are used to adjust and orient the polarization state of the incident light to ensure that the TFBG only works in one polarization state. The schematic structure of the optical setup is shown in Fig. 2. The insert gives the fabricated microfluidic chip.

Biomedical Optics EXPRESS

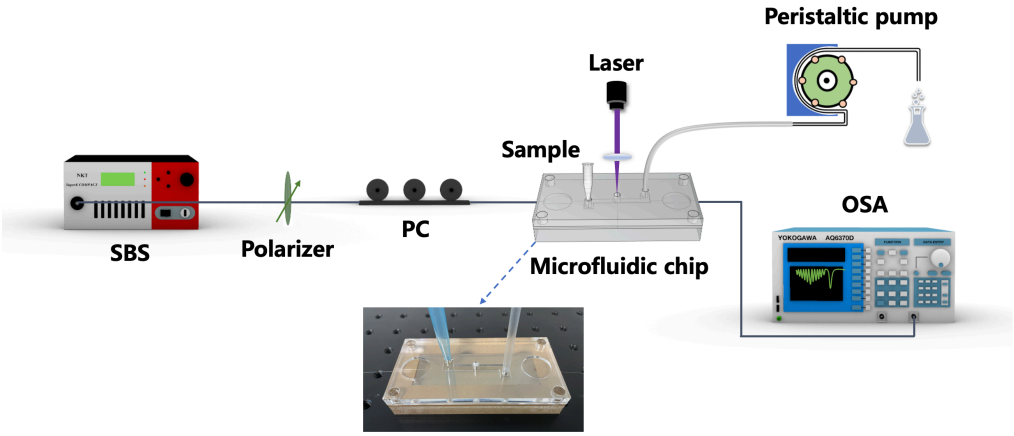

Fig. 2. Optofluidic system for pesticide detection based on photothermal spectroscopy.

3. Results and discussion

3.1. Characteristics of the MXene-TFBG

Figure 3(a) shows the scanning electron microscope (SEM) image of Nb_2CT_x MXene nanosheets (Nanjing Xianfeng Nano Material Technology Co. Ltd.). The few layers of Nb_2CT_x MXene are dispersed in NMP solvent, and the lateral size of the sheet is 1–7 μm, which is informed from the transmission electron microscope (TEM) image (Fig. 3(b)). The inset gives the magnified TEM image that shows the Nb_2CT_x MXene accumulation of different thicknesses, and the thickness of sheet is 1–5 nm. Figure 3(c) demonstrates the Raman spectrum of the Nb_2CT_x MXene, recorded by a Raman microscope (RENISHAW inVia Raman Microscope, 532 nm green light). The two Raman peaks of ω_1 and ω_2 corresponding to the in-plane oscillations of Nb and C atoms, which are characteristic of Nb_2CT_x [32].

We took optical microscope images of the TFBG surface before and after Nb_2CT_x MXene coating to confirm the decoration (OM, Olympus DSX1000). As shown in Fig. 3(d), the boundary between the fiber and the Nb_2CT_x MXene layer can be clearly distinguished. Figure 3(e) shows that the thickness of the deposited film is 395.2 nm (Dektak 150, Veeco). After Nb_2CT_x MXene coated on the surface of TFBG, the resonance intensity of the cladding mode decreases, as shown in Fig. 3(f). This phenomenon arises from the strong optical absorption of the Nb_2CT_x MXene.

3.2. Investigation of pesticide photothermal effect

Chlorpyrifos is an organophosphorus pesticide with good optical absorption characteristics in the range of 300 − 400 nm, as shown in Fig. 4(a) (UV-vis spectrometer UV-5100B). We choose a 400 nm laser source as the excitation light to irradiate the analyte and induce photothermal effect. According to the theoretical analysis in section 2.2, at a fixed concentration, the photothermal signal generated by the molecule is related to the power of the excitation light P_{exc} and the sample irradiation time t. With the increase of P_{exc} and t, the photothermal signal gradually increases, which amplifies the change in RI of the solution and improves the sensitivity of detection.

The chlorpyrifos solution with a concentration of 50 ppm flows into the microfluidic chip through a peristaltic pump. A 20 mW 400 nm laser is focused into the chip through a lens to excite the photothermal effect of the analyte. Continue to irradiate for 10 minutes, and record the TFBG transmission spectrum every 2 min (Fig. S1). The experimental results show that as the

Biomedical Optics EXPRESS

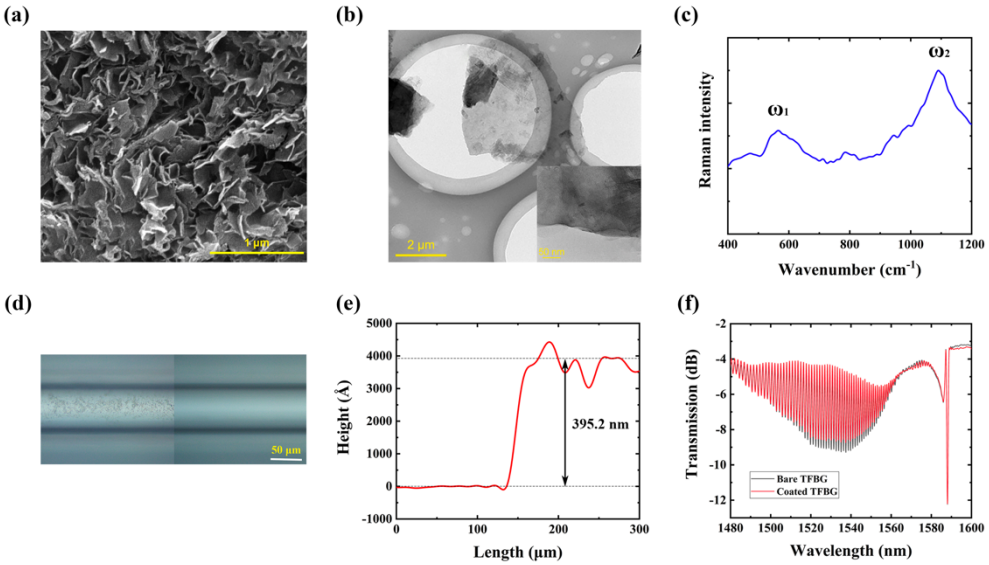

Fig. 3. (a) SEM image of Nb_2CT_x MXene dispersion. (b) TEM of Nb_2CT_x MXene nanosheets. Inset: magnified TEM image of Nb_2CT_x MXene nanosheets. (c) Raman spectrum of the Nb_2CT_x MXene. (d) Optical microscope images of the TFBG surface before and after Nb_2CT_x MXene coating. (e) Height profile alone the Nb_2CT_x MXene-TFBG. (f) Transmission spectrum of bare and coated TFBG.

irradiation time increases, the resonance wavelength shift of the TFBG cladding mode gradually increases, as shown in Fig. 4(b). Under laser irradiation, its resonance wavelength shifts to the long wavelength direction (red-shifts). This is due to the heat energy generated by the analyte absorbing light which increases the RI of the solution, resulting in an increase in the effective RI of the cladding mode. At the same conditions, the Nb_2CT_x MXene-TFBG was irradiated with excitation light, but the resonance wavelength of the cladding mode did not change. This indicates that the photothermal signal only comes from the analyte when detecting chlorpyrifos, and the photothermal signal produced by the molecule gradually increases with the improve of the irradiation time.

Furthermore, we investigated the influence of excitation light power on molecular photothermal effects. The excitation light with different power (0–20 mW) was used to irradiate 50 ppm chlorpyrifos solution, and record the change of TFBG transmission spectrum with laser power (Fig. S2). Figure 4(c) shows that the resonance wavelength of the TFBG cladding mode also red-shifts with the increase of laser power, and the offset is positively correlated with power. Therefore, we have verified that the photothermal effect of biomolecules becomes more obvious with the increase of irradiation time and excitation light power. Optimizing these two factors can enhance the photothermal signal produced by chlorpyrifos and increase the sensitivity of detection. The resonance wavelength shifted significantly when irradiated for 8 min, thus we chose to irradiate the sample with 20 mW 400 nm excitation light for 8 min to complete the subsequent detection of the chlorpyrifos.

3.3. Detection of pesticide

According to the photothermal research of chlorpyrifos, we found that the photothermal effect produced by the molecules absorbing photon energy can change the RI of the solution, thereby

Biomedical Optics EXPRESS

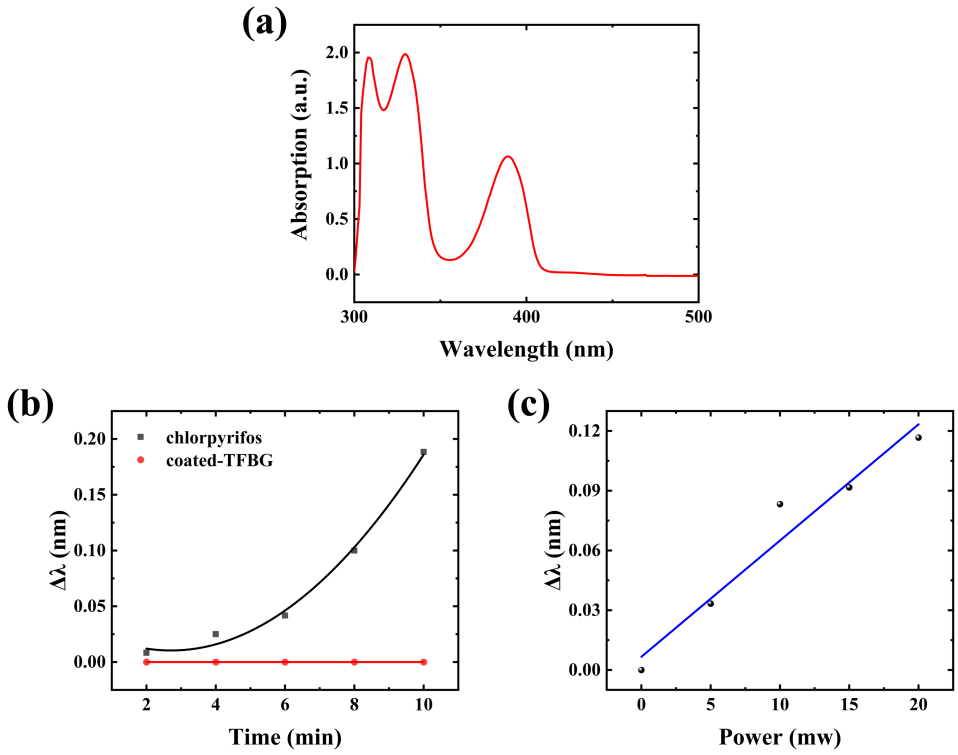

Fig. 4. (a) UV-Vis absorption spectrum of chlorpyrifos. The shift of TFBG resonance wavelength with (b) irradiation time and (c) excitation light power.

resulting the resonance wavelength of the TFBG cladding mode to shift. The RI of organophosphorus pesticides has a low correlation coefficient with concentration, thus the concentration of chlorpyrifos solution can be quantified based on photothermal principle.

When bare TFBG was used to detect chlorpyrifos, the transmission spectrum of TFBG in sample solutions of different concentrations (10 – 50 ppm) are shown in Fig. 5(a). Selecting the resonance wavelength at the "cut-off" point of the TFBG cladding mode for analysis, it is obvious that the transmission spectrum of TFBG has not shifted. In contrast, the resonance wavelength gradually red-shifted with the increase of analyte concentration when irradiated with excitation light, as shown in Fig. 5(b). It shows the TFBG transmission spectrum under different concentrations of chlorpyrifos solutions. The concentration coefficient of the organophosphorus pesticides RI is small, so there is no significant change in the low concentration range. Under the excitation light irradiation, the organophosphorus pesticide can absorb the photon energy and convert it into the photothermal signal, resulting a detectable change in the RI of the solution, and finally causing the resonance wavelength of the cladding mode to shift. Figure 5(c) plots the variation of resonance wavelength with concentration by data fitting, and compares the sensitivity of the two cases. The experimental results show that the sensitivity of TFBG is 1.3 pm/ppm when detecting the concentration of chlorpyrifos solution combined with the photothermal effect of the molecule.

Nb_2CT_x MXene is a two-dimensional material similar to graphene, with high specific surface area, hydrophilicity and biocompatibility. It can adsorb more molecules to be measured, thereby improving the sensing performance. Nb_2CT_x MXene was coated on the surface of TFBG

Biomedical Optics EXPRESS

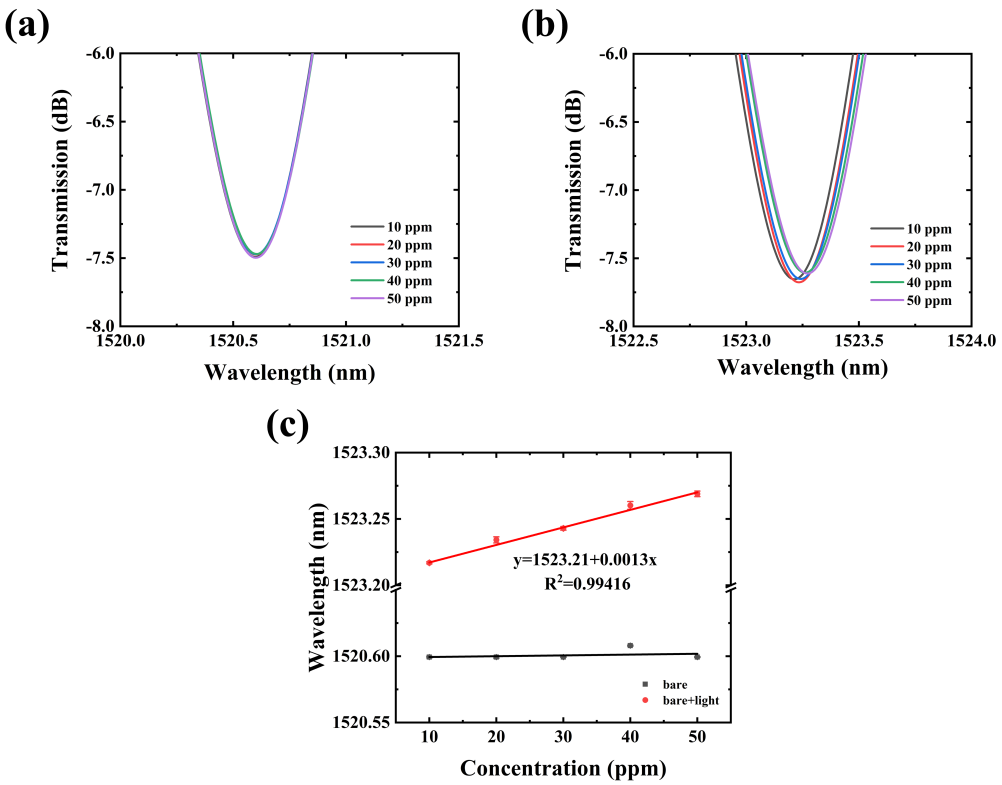

Fig. 5. The transmission spectrum of TFBG cladding mode in sample solutions of different concentrations under (b) irradiation and (a) without. (c) The sensitivity of chlorpyrifos detection under two cases.

by optical deposition method and used to detect chlorpyrifos sample solutions of different concentrations. Similarly, for Nb_2CT_x MXene-TFBG, the transmission spectrum of TFBG still has no significant shift (Fig. 6(a)), which further indicates the coefficient between the RI and concentration of organophosphorus pesticides. Figure 6(b) shows the change of TFBG transmission spectrum with chlorpyrifos concentration under the irradiation of 400 nm excitation light. It can be clearly seen that the resonance wavelength at the "cut-off" point of the TFBG cladding mode red-shifted with the increase of sample concentration, and the resonance intensity decrease. Furthermore, the resonance wavelength and intensity of the core mode keep constant, make it an ideal temperature reference. The detection sensitivity is improved to 1.8 pm/ppm and 0.0285 dB/ppm with the linearity of 0.95512 and 0.93946, as shown in Fig. 6(c). The limit of detection (LOD) of the chlorpyrifos was found to be as small as 0.35 ppm, which is far below the concentration lead to apoptosis of 18 mg/L [33]. A performance comparison of different methods for detecting chlorpyrifos is shown in Table 1. Using this method, real-time and accurate concentration detection of pesticide residues in food and soil can be performed.

3.4. Discussion of temperature and selectivity

In the detection of organophosphorus pesticides, the temperature change induced by the molecular photothermal effect is very small, so it is necessary to eliminate the influence of environmental temperature on the experimental results. The core mode of TFBG is inherently insensitive to the

Biomedical Optics EXPRESS

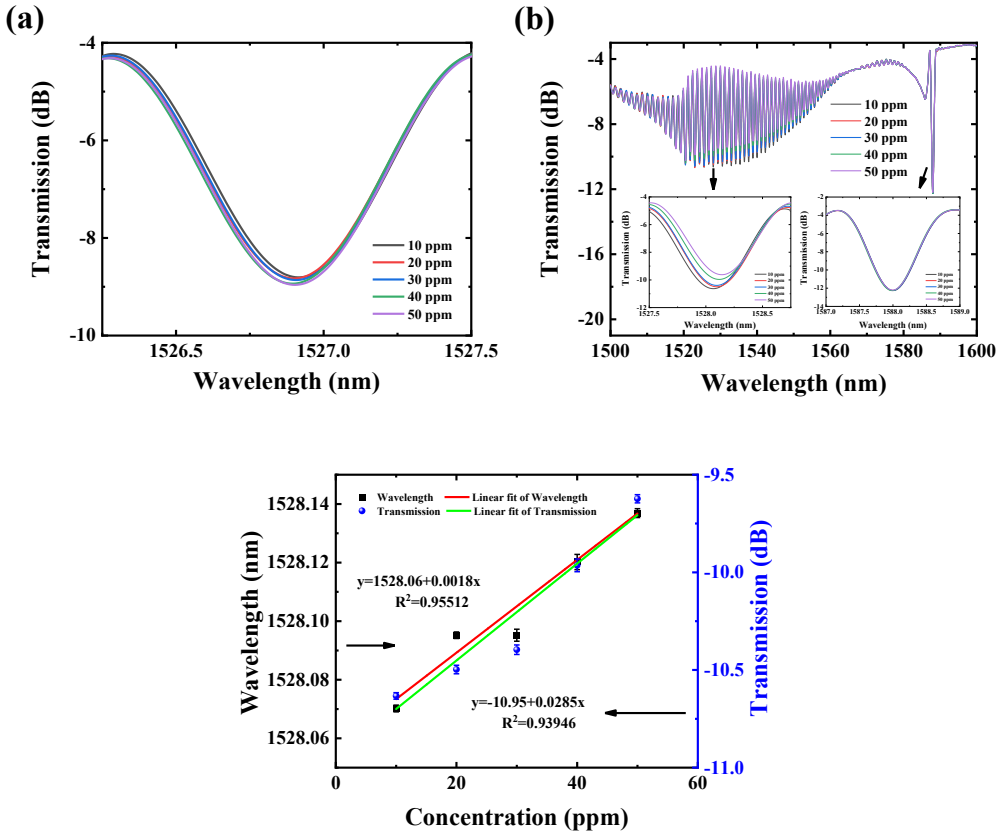

Fig. 6. The transmission spectrum of Nb_2CT_x MXene-TFBG in sample solutions of different concentrations (a) before and (b) after irradiation. (c) The sensitivity of chlorpyrifos detection under the irradiation.

Table 1. Performance comparison of the different methods for the detection of chlorpyrifos

Method	LOD (ppm)	Linear Range (ppm)	Temperature compensated	Ref
GC-MS	0.5	0.5–5	–	[6]
Electrochemistry	0.14×10^{-3}	0.02–0.1	–	[11]
Optical fiber	0.04	0.05–2	No	[34]
SPR	0.002	10–80	No	[14]
Infrared micro-imaging	0.98	100–10000	No	[35]
PTS based Nb_2CT_x -TFBG	0.35	10–50	Yes	This work

Biomedical Optics EXPRESS

RI, but similar to the cladding modes, it is sensitive to the temperature. Therefore, we can avoid the temperature effect by using spectral interrogation of core mode.

In order to investigate the temperature response of Nb_2CT_x MXene-TFBG, the prepared biosensor was placed in a temperature chamber, and recorded its transmission spectrum with the ambient temperature (Fig. 7(a)). The experimental results show that the resonance wavelength of TFBG red-shifted gradually with increase of temperature from 40 °C to 80 °C, and the temperature sensitivity of core mode and cladding modes are 8.72 pm/°C and 8.13 pm/°C, respectively (Fig. 7(b)). Combined with the experimental results in section 3.2, both the concentration of chlorpyrifos and temperature will cause the resonance wavelength of the cladding mode to shift. Therefore, the ambient temperature will produce experimental errors and affect the detection of chlorpyrifos. However, the core mode is only sensitive to temperature, and temperature compensation can be performed by referring core mode to avoid the influence of ambient temperature. The temperature induced concentration measurement error is 4.84 ppm/°C.

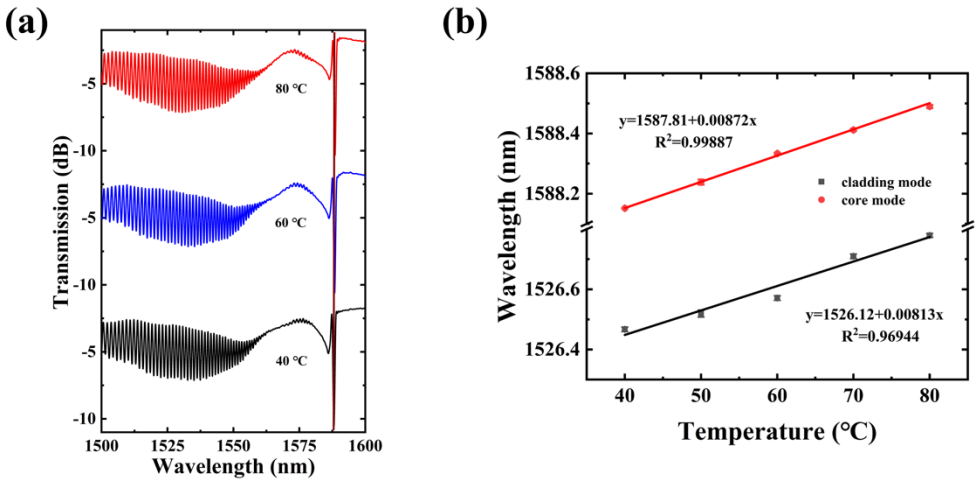

Fig. 7. (a) Temperature response of the Nb_2CT_x MXene-TFBG. (b) The temperature sensitivity of TFBG cladding mode and core mode.

The selectivity test was performed to exclude the influence of other interfering substances that may be contained in the pesticide. The proposed method was used to detect 50 ppm solutions of K^+, Na^+ and Ca^{2+}, and its selectivity was verified by comparing spectral responses, as shown in Fig. 8. The experimental results show that the chlorpyrifos solution induces a significant shift in the resonance wavelength of the cladding mode compared with the other three inorganic ions. This shows that the Nb_2CT_x MXene-TFBG biosensor based on the molecular photothermal effect exhibits selectivity and eliminate the influence of other potentially interfering substances. It is worth noting that the selectivity of photothermal spectroscopy comes from the optical absorption at specific wavelengths by the analyte [15]. This avoids the functionalization on the surface of the optical fiber, and effectively simplifies the operation difficulty of the experiment.

Biomedical Optics EXPRESS

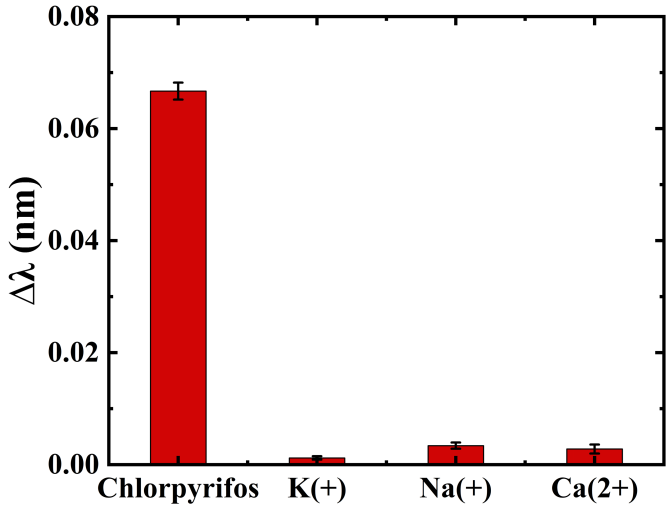

Fig. 8. Selectivity test of the Nb_2CT_x MXene-TFBG biosensor based on the molecular photothermal effect.

4. Conclusion

In conclusion, we have demonstrated a pesticide biosensor based on molecular photothermal effect using Nb_2CT_x MXene-TFBG. Under the excitation light irradiation, the photothermal effect of chlorpyrifos induce a detectable change of RI, resulting in the transmission spectrum of TFBG cladding mode changes. Nb_2CT_x MXene was coated on the surface of TFBG, allowing more molecules to be absorbed and enhancing the interaction between light and matter, which improves the sensitivity to 1.8 pm/ppm and 0.0285 dB/ppm. The LOD as low as 0.35 ppm. In addition, the influence of the ambient temperature is eliminated by detecting the change of TFBG core mode, and the obtained temperature compensation coefficient is 4.84 ppm/°C. The sensitivity can be improved by optimizing the deposition technique of integrating material and photothermal excitation conditions. This method exhibits many advantages of low LOD, specificity, temperature compensation, and real-time online monitoring, making it a good candidate for medical, chemical and environmental monitoring.

Funding. Guangdong Outstanding Scientific Innovation Foundation (2019TX05X383); Tianjin Research Innovation Project for Postgraduate Students (2020YJSS160); National Key Research and Development Program of China (2017YFB0405600); Natural Science Foundation of Tianjin City (17CZDJC31700, 17JCYBJC16100, 18JCZDJC30500, 20JCYBJC00300); National Natural Science Foundation of China (11874281, 11875032, 61975068, 62011530459, 62035006).

Disclosures. The authors declare that there are no conflicts of interest related to this article.

Data availability. Data underlying the results presented in this paper are not publicly available for privacy reasons, but may be obtained from the authors upon reasonable request.

Supplemental document. See Supplement 1 for supporting content.

References

1. M. A. Kamyabi and M. Moharramnezhad, "An enzyme-free electrochemiluminescence sensing probe based on ternary nanocomposite for ultrasensitive determination of chlorpyrifos," Food Chem **351**, 129252 (2021).
2. V. P. Androutsopoulos, A. F. Hernandez, J. Liesivuori, and A. M. Tsatsakis, "A mechanistic overview of health associated effects of low levels of organochlorine and organophosphorous pesticides," Toxicology **307**, 89–94 (2013).
3. F. Kamel and J. A. Hoppin, "Association of pesticide exposure with neurologic dysfunction and disease," Environ Health Perspect **112**(9), 950–958 (2004).

Biomedical Optics EXPRESS

4. S. Sun, V. Sidhu, Y. Rong, and Y. Zheng, "Pesticide Pollution in Agricultural Soils and Sustainable Remediation Methods: a Review," Current Pollution Reports **4**(3), 240–250 (2018).
5. J. Kaushal, M. Khatri, and S. K. Arya, "A treatise on Organophosphate pesticide pollution: Current strategies and advancements in their environmental degradation and elimination," Ecotoxicol Environ Saf **207**, 111483 (2021).
6. B. Y. P. Tay and W. H. Wai, "A gas chromatography–mass spectrometry method for the detection of chlorpyrifos contamination in palm-based fatty acids," J Am Oil Chem Soc **98**, 881–887 (2021).
7. G. Martinez-Dominguez, P. Plaza-Bolanos, R. Romero-Gonzalez, and A. Garrido-Frenich, "Analytical approaches for the determination of pesticide residues in nutraceutical products and related matrices by chromatographic techniques coupled to mass spectrometry," Talanta **118**, 277–291 (2014).
8. L. F. Melo, C. H. Collins, and I. C. Jardim, "High-performance liquid chromatographic determination of pesticides in tomatoes using laboratory-made NH2 and C18 solid-phase extraction materials," J Chromatogr A **1073**(1-2), 75–81 (2005).
9. J. Ye, J. Wu, and W. Liu, "Enantioselective separation and analysis of chiral pesticides by high-performance liquid chromatography," TrAC Trends in Analytical Chemistry **28**(10), 1148–1163 (2009).
10. J. S. Noori, J. Mortensen, and A. Geto, "Recent Development on the Electrochemical Detection of Selected Pesticides: A Focused Review," Sensors **20**(8), 2221 (2020).
11. F. O. Pelit, H. Ertaş, and F. Nil Ertaş, "Development of an adsorptive catalytic stripping voltammetric method for the determination of an endocrine disruptor pesticide chlorpyrifos and its application to the wine samples," J Appl Electrochem **41**(11), 1279–1285 (2011).
12. M. Ayat, K. Ayouz, C. Yaddadene, M. Berouaken, and N. Gabouze, "Porous silicon-modified electrode for electrochemical pesticide biosensor," J Coat Technol Res **18**(1), 53–62 (2021).
13. V. I. Chegel, Y. M. Shirshov, E. V. Piletskaya, and S. A. Piletsky, "Surface plasmon resonance sensor for pesticide detection," Sensors and Actuators B: Chemical **48**(1-3), 456–460 (1998).
14. Y. Wang, Z. Cui, X. Zhang, X. Zhang, Y. Zhu, S. Chen, and H. Hu, "Excitation of Surface Plasmon Resonance on Multiwalled Carbon Nanotube Metasurfaces for Pesticide Sensors," ACS Appl Mater Interfaces **12**(46), 52082–52088 (2020).
15. A. Vasiliev, A. Malik, M. Muneeb, B. Kuyken, R. Baets, and G. Roelkens, "On-Chip Mid-Infrared Photothermal Spectroscopy Using Suspended Silicon-on-Insulator Microring Resonators," ACS Sens. **1**(11), 1301–1307 (2016).
16. L. Pogačnik and M. Franko, "Detection of organophosphate and carbamate pesticides in vegetable samples by a photothermal biosensor," Biosens. Bioelectron. **18**(1), 1–9 (2003).
17. M. Sypabekova, S. Korganbayev, A. Gonzalez-Vila, C. Caucheteur, M. Shaimerdenova, T. Ayupova, A. Bekmurzayeva, L. Vangelista, and D. Tosi, "Functionalized etched tilted fiber Bragg grating aptasensor for label-free protein detection," Biosens Bioelectron **146**, 111765 (2019).
18. S. Cai, F. Liu, R. Wang, Y. Xiao, K. Li, C. Caucheteur, and T. Guo, "Narrow bandwidth fiber-optic spectral combs for renewable hydrogen detection," Sci. China Inf. Sci. **63**(12), 222401 (2020).
19. A. Lopez Aldaba, Á. González-Vila, M. Debliquy, M. Lopez-Amo, C. Caucheteur, and D. Lahem, "Polyaniline-coated tilted fiber Bragg gratings for pH sensing," Sensors and Actuators B: Chemical **254**, 1087–1093 (2018).
20. K. Zhou, L. Zhang, X. Chen, and I. Bennion, "Low Thermal Sensitivity Grating Devices Based on Ex-45 Tilting Structure Capable of Forward-Propagating Cladding Modes Coupling," J. Lightwave Technol. **24**(12), 5087–5094 (2006).
21. T. Guo, F. Liu, X. Liang, X. Qiu, Y. Huang, C. Xie, P. Xu, W. Mao, B. O. Guan, and J. Albert, "Highly sensitive detection of urinary protein variations using tilted fiber grating sensors with plasmonic nanocoatings," Biosens Bioelectron **78**, 221–228 (2016).
22. B. Jiang, X. Lu, X. Gan, M. Qi, Y. Wang, L. Han, D. Mao, W. Zhang, Z. Ren, and J. Zhao, "Graphene-coated tilted fiber-Bragg grating for enhanced sensing in low-refractive-index region," Opt. Lett. **40**(17), 3994–3997 (2015).
23. K. Zhang, Z. Fan, B. Yao, Y. Ding, J. Zhao, M. Xie, and J. Pan, "Exploring the trans-cleavage activity of CRISPR-Cas12a for the development of a Mxene based electrochemiluminescence biosensor for the detection of Siglec-5," Biosens Bioelectron **178**, 113019 (2021).
24. Y. Chen, Y. Ge, W. Huang, Z. Li, L. Wu, H. Zhang, and X. Li, "Refractive Index Sensors Based on Ti3C2Tx MXene Fibers," ACS Appl. Nano Mater. **3**(1), 303–311 (2020).
25. M. Wu, Q. Zhang, Y. Fang, C. Deng, F. Zhou, Y. Zhang, X. Wang, Y. Tang, and Y. Wang, "Polylysine-modified MXene nanosheets with highly loaded glucose oxidase as cascade nanoreactor for glucose decomposition and electrochemical sensing," J Colloid Interface Sci **586**, 20–29 (2021).
26. K. Deshmukh, T. Kovářík, and S. K. Khadheer Pasha, "State of the art recent progress in two dimensional MXenes based gas sensors and biosensors: A comprehensive review," Coord. Chem. Rev. **424**, 213514 (2020).
27. B. Gu, W. Qi, J. Zheng, Y. Zhou, P. P. Shum, and F. Luan, "Simple and compact reflective refractometer based on tilted fiber Bragg grating inscribed in thin-core fiber," Opt. Lett. **39**(1), 22–25 (2014).
28. T. Guo, F. Liu, Y. Liu, N. K. Chen, B. O. Guan, and J. Albert, "In-situ detection of density alteration in non-physiological cells with polarimetric tilted fiber grating sensors," Biosens Bioelectron **55**, 452–458 (2014).
29. Z. Zhang, K. Liu, J. Jiang, T. Xu, S. Wang, J. Ma, P. Chang, J. Zhang, and T. Liu, "Refractometric Sensitivity Enhancement of Weakly Tilted Fiber Bragg Grating Integrated with Black Phosphorus," Nanomaterials **10**(7), 1423 (2020).

Biomedical Optics EXPRESS

30. M. Yahya and M. Z. Saghir, "Empirical modelling to predict the refractive index of human blood," Phys. Med. Biol. **61**(4), 1405–1415 (2016).
31. W. Li, Y. Miao, C. Fei, H. Zhang, B. Li, and K. Zhang, "Enhanced photothermal signal detection by graphene oxide integrated long period fiber grating for on-site quantification of sodium copper chlorophyllin," Analyst **146**(11), 3617–3622 (2021).
32. Z. Yang, L. Gao, H. Chen, F. Zhang, Q. Yang, X. Ren, S. Zaheer, U. Din, C. Li, J. Leng, J. Zhang, Z. Lin, J. Wang, C. Li, and H. Zhang, "Broadband few-layer niobium carbide MXene as saturable absorber for solid-state lasers," Opt. Laser Technol. **142**, 107199 (2021).
33. Y. Zhang, Y. Chang, H. Cao, W. Xu, Z. Li, and L. Tao, "Potential threat of Chlorpyrifos to human liver cells via the caspase-dependent mitochondrial pathways," Food and Agricultural Immunology **29**(1), 294–305 (2018).
34. B. Kuswandi, C. I. Fikriyah, and A. A. Gani, "An optical fiber biosensor for chlorpyrifos using a single sol-gel film containing acetylcholinesterase and bromothymol blue," Talanta **74**(4), 613–618 (2008).
35. X. Li, D. Zhu, Z. Ma, L. Pan, D. Wang, and J. Wang, "Feasibility study of the detection of chlorpyrifos residuals on apple skin based on infrared micro-imaging," Opt. Eng **51**(10), 103204 (2012).